HHS Public Access

Author manuscript

Nature. Author manuscript; available in PMC 2018 December 06.

Published in final edited form as:

Nature. 2018 June ; 558(7709): 324–328. doi:10.1038/s41586-018-0183-2.

Dynamic allostery can drive cold adaptation in enzymes

Harry G. Saavedra[a,b], **James O. Wrabl**[a,b], **Jeremy A. Anderson**[a,b], **Jing Li**[a,b], and **Vincent J. Hilser**[*,a,b]

[a]Department of Biology, Johns Hopkins University, Baltimore, MD 21218

[b]T.C. Jenkins Department of Biophysics, Johns Hopkins University, Baltimore, MD 21218

Abstract

Adaptation of organisms to environmental niches is a hallmark of evolution. One prevalent example is that of thermal adaptation, wherein two descendants evolve at different temperature extremes[1,2]. Underlying the physiological differences between such organisms are changes in enzymes catalyzing essential reactions[3], with orthologues from each organism undergoing adaptive mutations that preserve similar catalytic rates at their respective physiological temperatures [4,5]. The sequence changes responsible for these adaptive differences, however, are often at surface exposed sites distant from the substrate binding site, leaving the active site of the enzyme structurally unperturbed[6,7]. How such changes are allosterically propagated to the active site, to modulate activity, is not known. Here we show that entropy-tuning changes can be engineered into distal sites of *Escherichia coli* adenylate kinase (AK) to quantitatively assess the role of dynamics in determining affinity, turnover, and the role in driving adaptation. The results not only reveal a dynamics-based allosteric tuning mechanism, but also uncover a spatial separation of the control of key enzymatic parameters. Fluctuations in one mobile domain (*i.e.* the *LID*) control substrate affinity, while dynamic attenuation in the other (*i.e.* the *AMPbd*) affects rate-limiting conformational changes governing enzyme turnover. Dynamics-based regulation may thus represent an elegant, widespread, and previously unrealized evolutionary adaptation mechanism that fine-tunes biological function without altering the ground state structure. Furthermore, because rigid-body conformational changes in both domains were thought to be rate limiting for turnover[8,9], these adaptation studies reveal a new paradigm for understanding the relationship between dynamics and turnover in AK.

Keywords

cold adaptation; dynamics; evolution; allostery; local unfolding

[*]Correspondence and Materials: hilser@jhu.edu, Tel: 410-516-6072; Fax: 410-516-5213.

Supplementary Information is linked to the online version of the paper at www.nature.com/nature.

Author Contributions

H. G. S. designed research, performed experiments, analyzed data, interpreted results, discussed research, and wrote the manuscript. J. O. W. analyzed data, interpreted results, discussed research, and wrote the manuscript. J. A. A. performed experiments, analyzed data, interpreted results, and discussed research. J. L. designed research and discussed research. V. J. H. designed research, analyzed data, interpreted results, discussed research, and wrote the manuscript.

The authors declare no competing financial interests.

AK catalyzes the reversible Mg^{2+}-dependent phosphoryl transfer reaction ATP +AMP↔2ADP, essential for *E. coli* survival[10]. AK contains three domains, canonically named *CORE* (residues 1–29, 74–121, and 160–214, figure 1a), *AMPbd* (30–73), and *LID* (122–159). *CORE*, which positions the catalytic residues critical to phosphoryl transfer, is the most stable domain and forms a majority of the binding site at which the transfer occurs[11,12]. Consistent with numerous structures in the Protein Data Bank, wherein isolated domains exhibit conformational changes sufficient to limit access to and from the active site in the bound complex (Extended Data figures 1&2, and SI tables S6&S7), flexible *LID* and *AMPbd* domains in AK undergo fluctuations that become spatially restricted during binding, remaining dampened until product release. Although these large conformational changes are often modeled as rigid-body motions[13,14], recent studies reveal that the *LID* undergoes uncorrelated sub-global motions for the entire group of residues comprising the *LID*[15–18], a process akin to 'local unfolding'.

To isolate the functional effects of local unfolding, allosteric mutation sites were selected to increase the probability of local unfolding, while preserving the ground state structure (Extended Data figure 3). Using strict criteria (Methods), solvent-exposed sites distal to the active site were targeted for mutation to Gly. Positions A37 and A55 were identified in *AMPbd*, and V135 and V142 were identified in *LID* (figure 1a). If the conformational fluctuations involving those regions were indeed local unfolding, Gly mutations would increase the number of backbone conformations in those states. The maximum expected increase is ~3.4 to 4.5-fold for positions that are Ala and Val, respectively, stabilizing the locally unfolded states by ~730 and 910 cal/mol[19,20] and increasing their probability (figure 1b). Alternatively, if locally unfolded states are not already marginally probable in WT, stabilizing such states by ~ 1.0 kcal/mol should have no impact. Thus, this strategy is a direct probe of functionally important locally unfolded states in both the *LID* and the *AMPbd*.

The conformational stability and dynamics of each Gly mutant was investigated using differential scanning calorimetry (DSC) (figure 2a, Extended Data figure 4). *LID* and *AMPbd* mutations affected AK differently, with a significant diminution in the area of the main unfolding transition and the appearance of a low temperature peak in the *LID* mutations (figure 2a). Fitting of the data (Extended Data figure 5 and Extended Data table 1) indicates the origin of the effect is an intermediate (*i.e.*, *I*-state), which is 5% populated at physiological temperature for WT (37°C) and is increased to ~40% in the *LID* mutants (figure 2b), consistent with previous circular dichroism (CD) and isothermal titration calorimetry (ITC) results[15]. To the contrary, mutations in the *AMPbd* show no effect on the *I*-state at 37°C (figure 2c).

Importantly, because the *LID* comprises part of the binding site, the *LID*-unfolded *I*-state should display decreased affinity relative to the fully folded *N*-state. If so, mutations that destabilize the *LID* and increase the probability of the *I*-state should decrease the affinity of AK for ligand. Consistent with this prediction, ITC experiments that monitored the binding of the WT and the mutant AKs to the bi-substrate analog Ap5A (Extended Data figure 6) revealed that while the affinity of the *LID* mutants is decreased relative to WT, as shown

previously[15], the *AMPbd* mutations have no effect on affinity. Furthermore, inspection of binding enthalpies (*i.e.* ΔH_b) from ITC (figure 2d), corroborates this model and reconciles the thermodynamics of binding with the thermodynamics of the conformational changes observed from DSC (figures 2a–c). Thus, the ITC and DSC results provide a self-consistent picture of the AK ensemble. Namely, at physiological temperature, the *LID* domain is unfolded 5% of the time, effectively modulating substrate affinity, while the *AMPbd* plays no role in modulating affinity.

The relationship between the thermodynamics and conformational dynamics was further investigated using nuclear magnetic resonance (NMR). Relaxation studies of the ligand bound (*i.e. holo*) form of AK implicate *LID* conformational fluctuations to be rate-limiting for enzyme turnover[8,21,22]. To determine the nature of conformational fluctuations affecting affinity, backbone dynamics were measured for the ligand-free (*i.e. apo*) forms using ^{15}N Carr-Purcell-Meiboom-Gill (CPMG) NMR relaxation dispersion experiments[23,24], which provide direct access to processes occurring on the milli- to micro-second timescale. Previously, we showed that at 19°C the single *LID* mutation V142G has a similar population of the *LID* unfolded *I*-state to the WT protein at 37 °C[15,16,20]. The lower temperature thus permits direct comparison of *LID* fluctuations between the WT and all mutants.

As expected, the chemical shifts for *LID* residues showed conformational exchange in LID mutants, while the fluctuations of the remaining positions in the protein (with the exception of *CORE* residues 6 and 10, proximal to the *LID*) showed no exchange, resembling WT (figure 3a). Importantly, the population of the *LID*-unfolded state determined from the fit of the CPMG data (either individually or globally[16], P_I = 3–9%) agrees quantitatively with the population of the *LID*-unfolded state determined calorimetrically ($P_I \approx 5\%$). The fact that three independent techniques (*i.e.* ITC, DSC and NMR), each sensitive to different properties of the protein, yielded similar results supports a model whereby unfolding of the *LID* (instead of a rigid-body opening of an always-folded *LID*) is the minor conformational state of the *apo* protein regulating substrate affinity. In contrast, analysis of the ^{15}N NMR relaxation dispersion data for the *AMPbd* mutants showed no such effect (figure 3a), consistent with the fact that these mutants do not affect the substrate binding of AK.

To determine the relationship between conformational dynamics and activity, turnover was measured as a function of temperature for each mutant (figure 3b, Methods and SI table S3). As expected, the activity of each mutant increased until reaching a rollover temperature, after which the activity decreased due to denaturation (figure 3b). Paradoxically, while the single *LID* mutants each destabilized the *LID* (figures 2a&b) and increased its dynamics (figure 3a), such changes had no impact on the activity (k_{cat}) of AK (figure 3b). In contrast, single *AMPbd* mutants, which affected neither the stability (figures 2a&c) nor the dynamics (figure 3a), significantly *increased* the k_{cat} at every temperature (figure 3b). In other words, the dynamics and stability of the *LID* domain, and therefore the affinity, are uncoupled from the activity of the enzyme.

Further analysis of the activity using the method of Eyring[25] provides mechanistic insight into the role of unfolding in AK activity (figure 4). The activation enthalpy, which is proportional to the slope of rate constant versus inverse temperature, is identical between the

WT and all four single mutants (ΔH^t ~ 10.5 kcal/(mol*K). Indeed, the major difference between mutants is the average activation entropy ΔS^t (*i.e.* intercepts of the lines in figure 4), which for the *AMPbd* mutants is lower than the WT and *LID* mutants, increasing the catalytic rate at every temperature. The similarity in activation enthalpy suggests that the degree of structural change associated with the transition state is identical for the WT and all four mutations, but that the free energy difference is less for the two *AMPbd* mutations, with the difference being almost entirely entropic. Remarkably, the difference between the *AMPbd* mutations and the WT and *LID* mutants is $\Delta\Delta S^t$ = 2.5 cal/(mol*K) (figure 4, inset), corresponding to a change in activation energy, $\Delta\Delta G^t$ at 25 °C of approximately 770 cal/mol, which is the expected result if the rate-limiting transition state for product release is in fact a locally unfolded state of the *AMPbd* (see figure 1b).

The quantitative agreement with theoretical expectations for two different surface exposed positions in the *AMPbd* supports an interpretation that conformational change in *AMPbd*, but not the *LID*, is the rate-limiting step in product release for AK. Importantly, the nature of the *AMPbd* conformational change is also local unfolding, but because the unfolding in *AMPbd* is extremely rare, the millisecond timescale dynamics are unaffected. There is no evidence that the chemistry of the catalytic event is affected by local unfolding[26] (nor is it likely based on the nature of the surface mutations), but merely the rate-limiting product release step. Interestingly, these results also provide insight into thermo-adaptation studies of Nguyen, *et al.*[27], who report that increased curvature in Eyring plots is a signature of increased transition-state heat capacity in ancestral warm-adapted AK variants. The origin of this effect could involve local unfolding, although a definitive claim awaits further study.

For more than a century[28], biochemists have used the Arrhenius equation, $k = A \exp(-E_a / RT)$, to characterize temperature effects on enzyme reaction rates. This expression reveals that the reaction rate k increases exponentially with temperature, with the increase determined by the activation energy E_a (where R is the gas constant and A is a reaction-specific pre-exponential term). For typical activation energies, the rate increases approximately two-fold for every 10 °C environmental temperature rise. If such a model sufficiently describes activity, an enzyme from a psychrophilic organism (*e.g.* thrives at ~ 0 °C) should have activity more than 20 times lower than an orthologous enzyme from a mesophilic organism (*e.g.* thrives at ~ 40 °C). This, however, is not the case[7]. In several well-documented examples, it has been shown that although the activity of each orthologous enzyme obeys an Arrhenius relationship, increasing with temperature, the enzymes evolved such that the respective k_{cat} and K_m values are similar at the physiological temperature of each organism[4,5]. Clues to the origin of this effect can be gleaned from sequence analysis. Indeed, in studies of lactate dehydrogenase from a series of notothenioid fish adapted to different environmental temperatures[6], Fields and Somero found no changes to active site residues, but instead identified Gly to be prevalent at surface sites in cold adapted species, a result in agreement with the observations reported here for AK. In fact, the mechanism of this type of adaptive tuning can now be directly dissected.

Our results indicate that unfolding in both the *LID* and *AMPbd* contributes to function, although the specific roles are segregated in AK (figure 5). *LID* unfolding modulates the affinity of the enzyme for substrate (figure 5b) and is thus tuned to a level of ~5% for the

wild type. As local unfolding is favored entropically[19,20], mutation from a bulky side-chain (*e.g.* Val), which is restricted in unfolded state conformational accessibility, to Gly (figure 1b), stabilizes the *LID*-unfolded state to a level of ~40% (figure 5b–Step 1). Because unfolding is high-enthalpy, and disfavored at lower temperatures[19,20], a decrease in temperature resets the *LID*-unfolded equilibrium to the original level (figure 5b–Step 2). Unfolding in *AMPbd*, on the other hand, modulates the rate limiting process for turnover, utilizing the same principles at play in the *LID*. Mutations from Ala to Gly (figure 1b), increase the stability of the locally unfolded state of *AMPbd*, lowering the activation barrier for product release, and increasing the apparent rate (figure 5c–Step 1). As local unfolding in *AMPbd* is the rate-limiting step, mutation to Gly lowers the activation barrier for product release. Lowering temperature again dampens fluctuations, resetting the transition state equilibrium, and lowering the activity to the original level (figure 5c–Step 2).

Taken together, the results reveal that affinity and turnover in AK can be independently regulated through these similar, but spatially distinct, dynamic allosteric mechanisms. Illustrating this point, relative affinity and activity (figures 5b&c, respectively) are displayed for the WT and each of the mutants. Figure 5d reveals that the independent regulation is physiologically significant, as a single point mutation can substantially change one function (>30 %) while leaving the second function comparatively unaltered (<10 %), resulting in as much as a 10 °C downward shift in adaptive temperature. To our knowledge, such spatially segregated and dynamic (*i.e.* entropic) regulation of multiple functions within the same enzyme has yet to be documented.

The results described here for AK also suggest a general strategy for adaptation. By employing unfolded states, adaptation can be facilitated by introducing as few as one conformational entropy enhancing mutation anywhere on the surface of the protein structure that becomes unfolded. Such changes would energetically oppose the increased stability of the folded state of any domain that results at lower temperatures. Considering that the enrichment of flexibility-promoting residues in psychrophilic enzymes has long been identified from sequence analysis[6,29], it is possible that the local unfolding mechanism identified here is driving cold adaptation in numerous systems, even where structural data exists supporting alternative hypotheses, as shown here for AK[13,14] (Extended Data figures 1&2). Indeed, the Protein Data Bank contains numerous ligand-bound (*holo*) structures wherein the active site occludes the ligand, and the structural transitions associated with the substrate gaining access to and from the active site are, as yet, unknown (SI table S7, Extended Data figure 7, SI table S6), leaving open the possibility of local unfolding.

Finally, utilizing local unfolding as a mechanism for regulating key enzymatic parameters such as K_m and k_{cat} confers an additional potential advantage to organisms. Because the chaperone machinery has evolved to recognize unfolded states of proteins[30], utilization of local unfolding as part of the functional energy landscape provides an opportunity to tie the overall regulation of enzymes to the proteostatic state of the cell, and thus, indirectly, to any process that is co-regulated with chaperone activity. The validity of this hypothesis is currently under investigation.

Online Methods

Identification of entropy-enhancing mutation sites

Mutation sites were objectively identified based on a strict set of geometric criteria, to isolate positions distal to the active site that also had no side chain enthalpic interaction in the folded structure. These criteria were as follows: 1) the side chain of a mutated position should be highly surface exposed and devoid of intramolecular contacts, 2) the mutated side chain should not have polar or charged groups that could be involved in long-range interactions, 3) the mutated side chain should be distant (*i.e.* > 8 Å) from the active site, 4) the side chain should not make contact with the ligand. All these criteria were satisfied for all mutated positions in both the open (4ake.pdb[31]) and closed (1ake.pdb[32]) states of *WT* AK. Exactly four positions in the *LID* domain (V127, V135, V142, V148), and two positions in the *AMPbd* domain (A37, A55) were identified. Thus, the reported results pertain to the majority of all possible entropy enhancing mutations for this enzyme.

Protein mutagenesis and purification

WT AK amino acid sequence contained no affinity tag and was identical to Schrank, *et al.*[33]. The gene corresponding to this sequence was codon-optimized, synthesized, and inserted into an IPTG-inducible *pJ414* bacterial expression vector conferring ampicillin resistance (DNA 2.0, Menlo Park CA). This DNA template was used to make the single Gly variants using PCR site-directed mutagenesis. The AK-containing plasmid was used to transform *Rosetta2(DE3)pLysS Singles J* competent cells (Novagen EMD Millipore, Billerica MA). Protein was produced from batch cultures grown in 2xYT medium containing 60 μg/mL ampicillin. Protein was purified from sonicated *E. coli* lysate under native conditions using FPLC. AK for all variants was at least 95% pure as assayed by 12% SDS-PAGE. Full details of expression, purification, and handling are given in Supplementary Information[33].

Differential Scanning Calorimetry and Isothermal Titration Calorimetry

For DSC, 20 μM protein was measured in calorimetric buffer (60 mM PIPES, 1 mM EDTA, pH 7.2). A *MicroCal VP-DSC* (Malvern, Westborough MA) was set at: 10 °C start, 80 °C final, 60 °C/hr scan rate, 15 min prescan thermostat, 0 min postscan, 20 s filtering period, no feedback mode/gain. For ITC, 40 μM protein was measured in calorimetric buffer. Initial Ap5A inhibitor (Sigma-Aldrich, St. Louis MO) was 400 μM in calorimetric buffer. A *MicroCal VP-ITC* was set at: 55 total injections, 5 μL volume, 220 or 300 s spacing, 10 s duration, 2 s filter period, 307 rpm stir speed, high feedback mode/gain. Full details are given in Supplementary Information.

Kinetic measurements

k_{cat} in reverse direction was measured by coupled formation of $Mg^{2+}ATP$ to hexokinase (HK) and glucose-6-phosphate dehydrogenase (G6PDH) reactions[34]. Reaction mixture was 50 mM HEPES, 10 mM D-Glucose, 20 mM $MgCl_2$, 100 mM KCl, 15 mM ADP, 1.2 mM NADP, 0.5 mg /mL BSA, 10 U/mL each HK and G6PDH diluted in 50% w/v glycerol, pH 8.0. This mixture was equilibrated for 5 minutes and the reaction was started with 10 μL of 0.4 μM AK. Total volume was held constant at 1 mL. Rate of increase in 340 nm absorbance

measured NADPH formation. The linear portion of the activity was interpreted with Eyring analysis[34–36]. Full details are given in Supplementary Information.

Nuclear Magnetic Resonance spectroscopy

Successful transformants of AK constructs were subjected to a double colony selection to ensure robust expression in 100% D_2O MOPS minimal media[37], supplemented with 0.4% $^{2}H/^{12}C$ or $^{2}H/^{13}C$ glucose. Purification was performed as described above; AK was concentrated to 1mM in NMR sample buffer (50 mM HEPES, 20 mM $MgCl_2$, 5 mM TCEP, pH 7.0). Most assignments for all variants were conservatively transferred from previously reported spectra[33]. Relaxation-dispersion experiments[38] used a pulse sequence[39] with 50 ms constant time at 800 MHz field, with data collected at relaxation delays of 9.55, 0.25, and 0.0 (I_0) ms. TROSY-HSQC spectra were collected in an interleaved manner with 16 transients, 90 ms T1, and 2.5 s delay between transients for each relaxation delay at 19°C. R_2 values[40] were calculated from differences of peak intensities. Full details of NMR data acquisition, processing, analysis, and interpretation are given in Supplementary Information.

Ensemble model and estimation of conformational population

The Ensemble Allosteric Model[41] used experimentally determined stabilities and domain interaction energies (Extended Data table 1) to compute Boltzmann-weighted temperature-dependent AK ensemble populations (Main Text figures 2b&c). Three thermodynamic states were permitted: fully folded (P_F), binding incompetent locally unfolded LID (P_{LID}), and fully unfolded (P_U). Full details are given in Supplementary Information.

Statistical information

In all figures, error bars indicate the standard deviation around the mean value for at least three independent data points. There is one exception, Main Text figure 5d, where the bars are derived from propagation of errors between differences of mutant and WT activity and affinity measurements (which are explicitly reported in Supplementary Information).

Extended Data

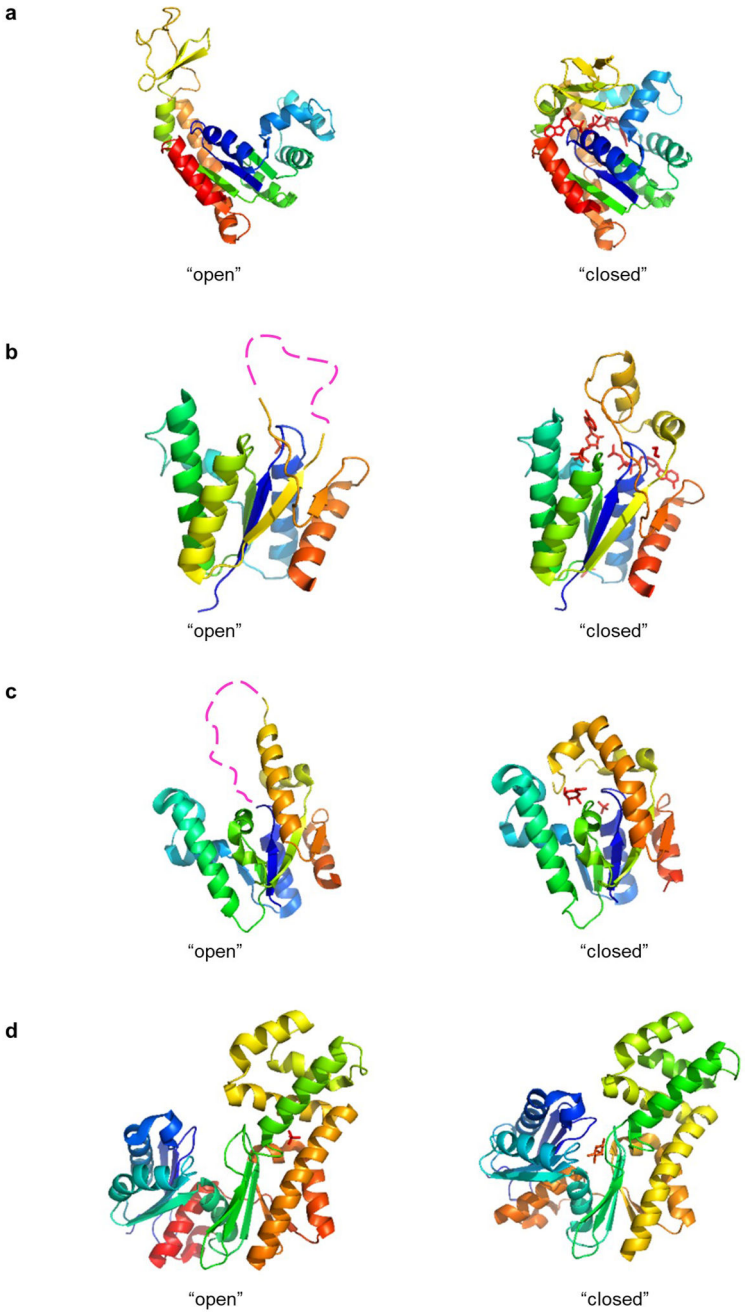

Extended Data Figure 1. Kinases of known structure that may exhibit similar open/close architecture as *E. coli* adenylate kinase

In each panel, the left cartoon represents a putative "lid open" *apo*-structure, and the right panel represents a putative "lid closed" *holo*-structure. Protein chains are rainbow-colored from blue (N-terminus) to red (C-terminus). Note that in panels b and c there is crystallographic evidence of disorder (magenta) in the conformationally changing "lid" domain, a situation very much like that seen for the low-population locally unfolded state in *E. coli* adenylate kinase, given in panel a for comparison. **a**. *E. coli* adenylate kinase: PDB

identifiers 4ake (left) and 1ake (right). **b**. *M. tuberculosis* adenylyl-sulfate kinase: PDB identifiers 4rfv (left) and 4bzx (right). **c**. *H. pylori* shikimate kinase: PDB identifiers 1zuh (left) and 1zui (right). **d**. *S. tokodaii* hexokinase: PDB identifiers 2e2n (left) and 2e2o (right).

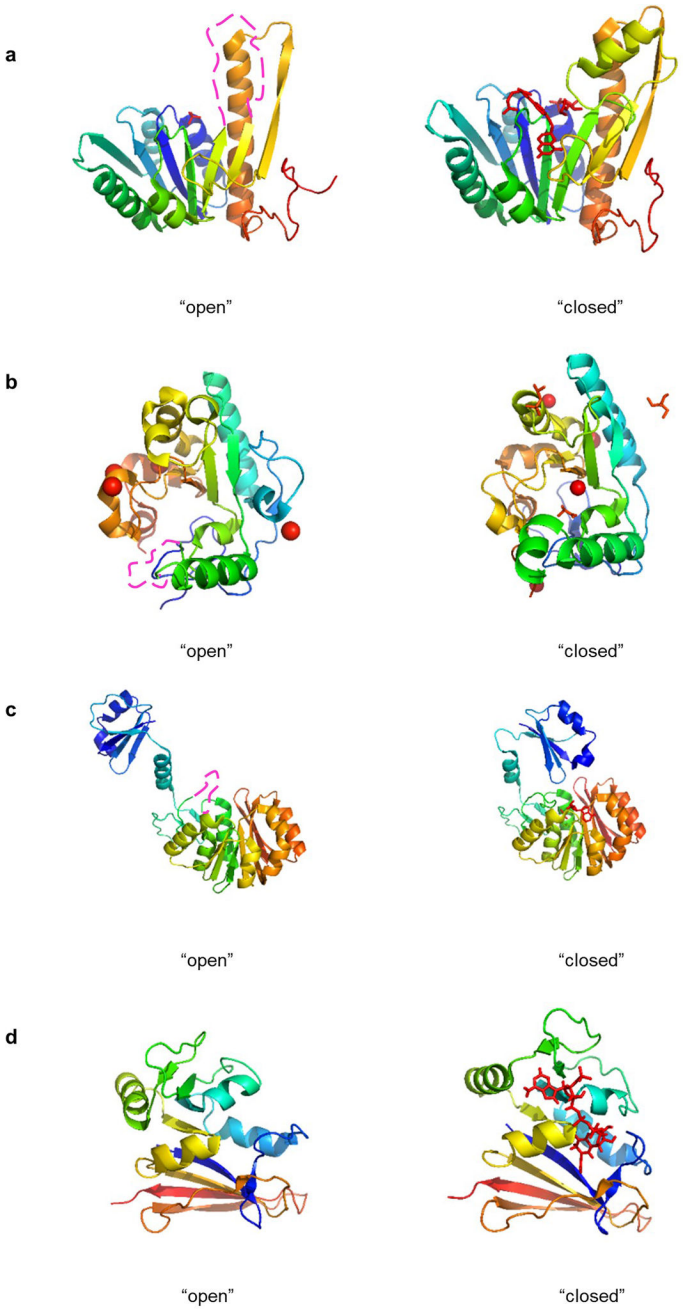

Extended Data Figure 2. Other enzymes of known structure that may exhibit similar open/close architecture as *E. coli* adenylate kinase

In each panel, the left cartoon represents a putative "lid open" *apo*-structure, and the right panel represents a putative "lid closed" *holo*-structure. Protein chains are rainbow-colored from blue (N-terminus) to red (C-terminus). Note that in panels a, b, and c there is

crystallographic evidence of disorder (magenta) in the conformationally changing “lid” domain, a situation very much like that seen for the low-population locally unfolded state in *E. coli* adenylate kinase. **a**. *E. coli* 2-glycinamide ribonucleotide transformylase: PDB identifiers 1cdd (left) and 1cde (right). **b**. *L,D*-carboxypeptidase: PDB identifiers 4jid (left) and 4ox5 (right). **c**. *T. thermophilus* ribosomal protein L11 methyltransferase Prma: PDB identifiers 2nxc (left) and 2nxe (right). **d**. *L. casei* dihydrofolate reductase: PDB identifiers 1l7o (left) and 2hqp (right).

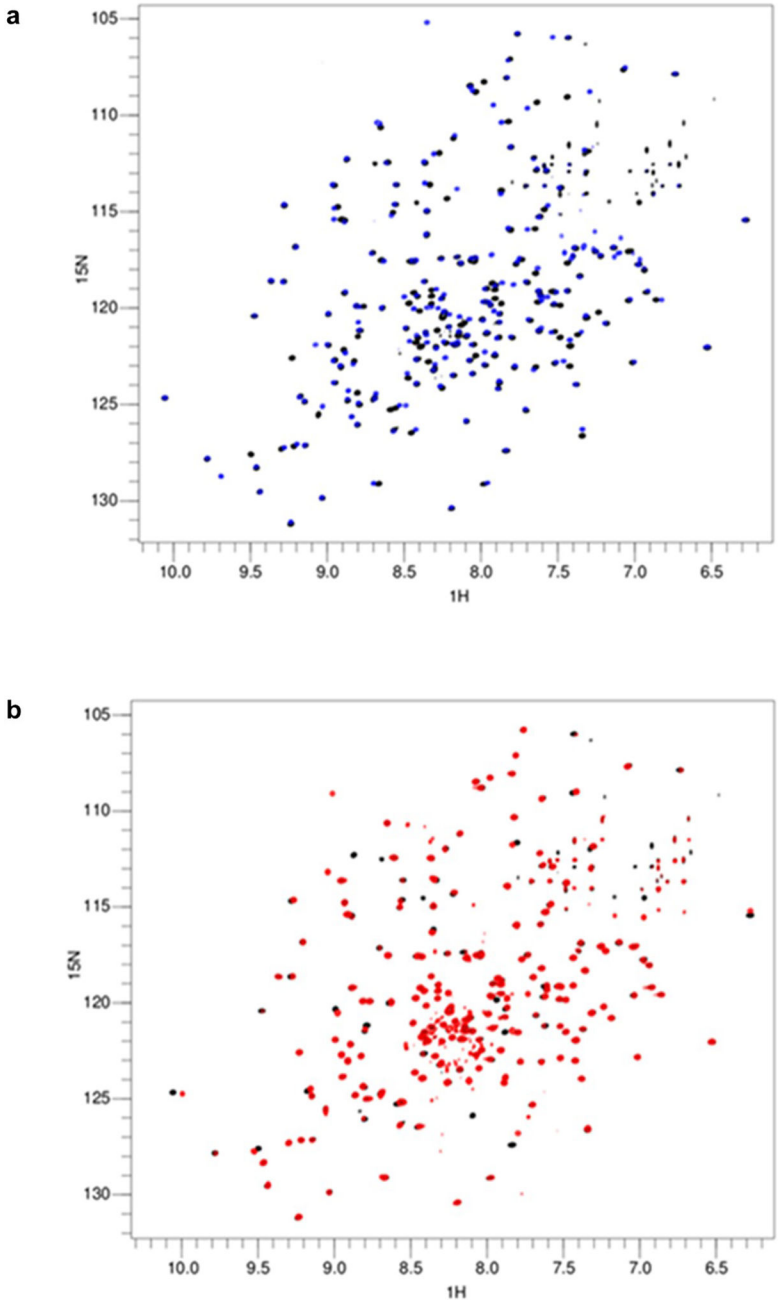

Extended Data Figure 3. Comparison of WT AK HSQC spectrum with A55G and V142G

Overlay HSQC spectra at 19 °C for A55G (blue, **a**) and V142G (red, **b**); in both panels an identical WT spectrum is shown in black. Peak dispersion in all spectra is consistent with folded protein and also is not inconsistent with a similar ground state structure shared among all three proteins. Individual resonances for both mutants exhibited minimal shifts from WT, and thus generally permitted transference of assignments from the WT.

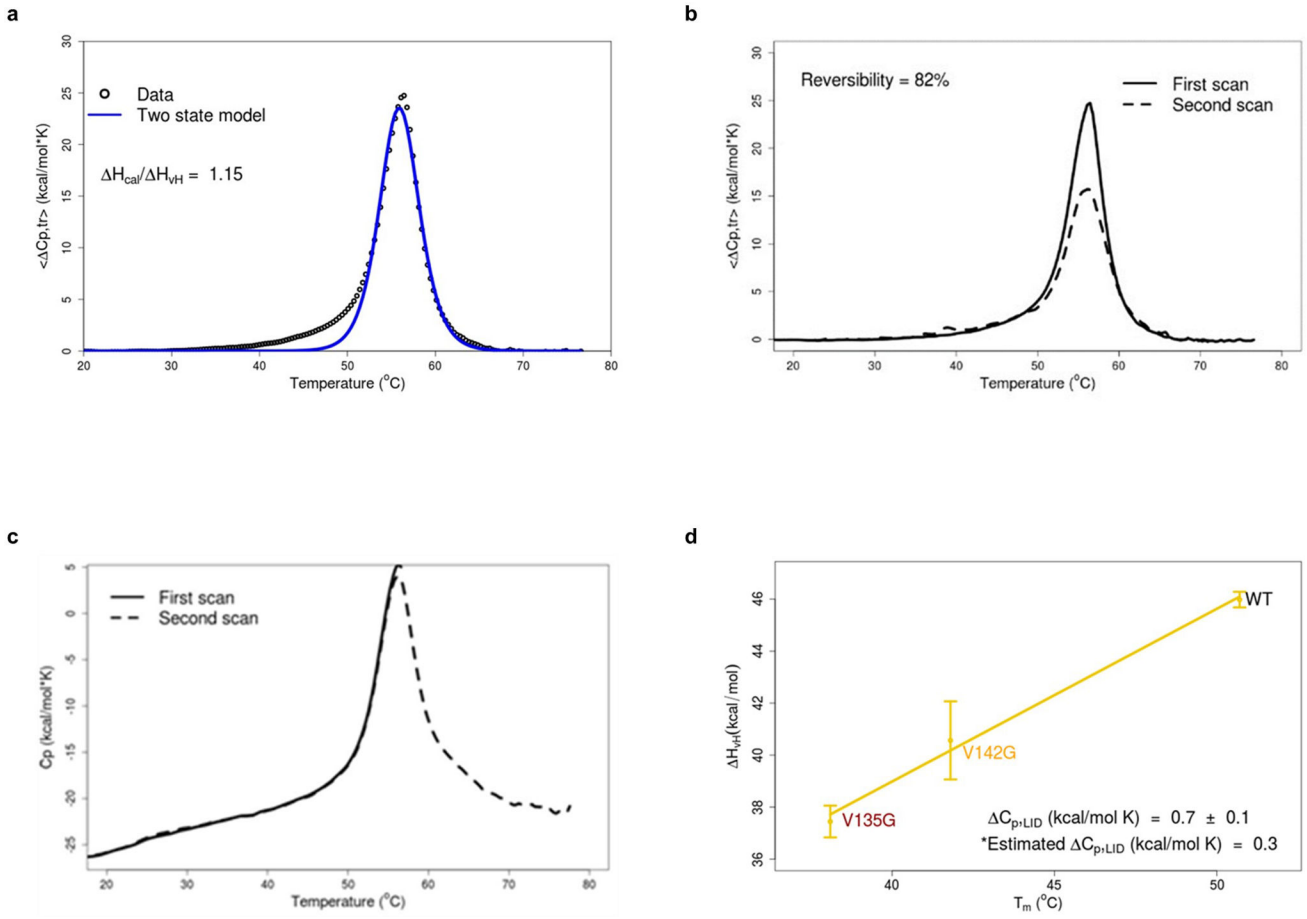

Extended Data Figure 4. DSC control experiments

a. Test of the two-state model using WT AK. WT thermal denaturation is not consistent with a two-state process, as data simulated under the two-state assumption does not agree with experiment, and calorimetric to van't Hoff enthalpy ratio is substantially greater than 1. Results represent $n = 1$ independent experiments. **b**. Reversibility test. WT AK exhibited approximately 80% of the original calorimetric area upon re-heating. Results represent $n = 1$ independent experiments. **c**. High temperature test. WT AK demonstrates complete reversibility when extreme high temperature is avoided. Results represent $n = 1$ independent experiments. **d**. Calorimetric heat capacity ΔC_p of AK *LID* variants. Dependence of enthalpy on melting temperature for WT, V135G, and V142G results in $\Delta C_{p,LID}$ of 0.7 +/− 0.1 kcal/mol K. This value is reasonably consistent with energetics determined from accessible surface areas. Results represent mean +/− s.d. of $n = 3$ independent experiments.

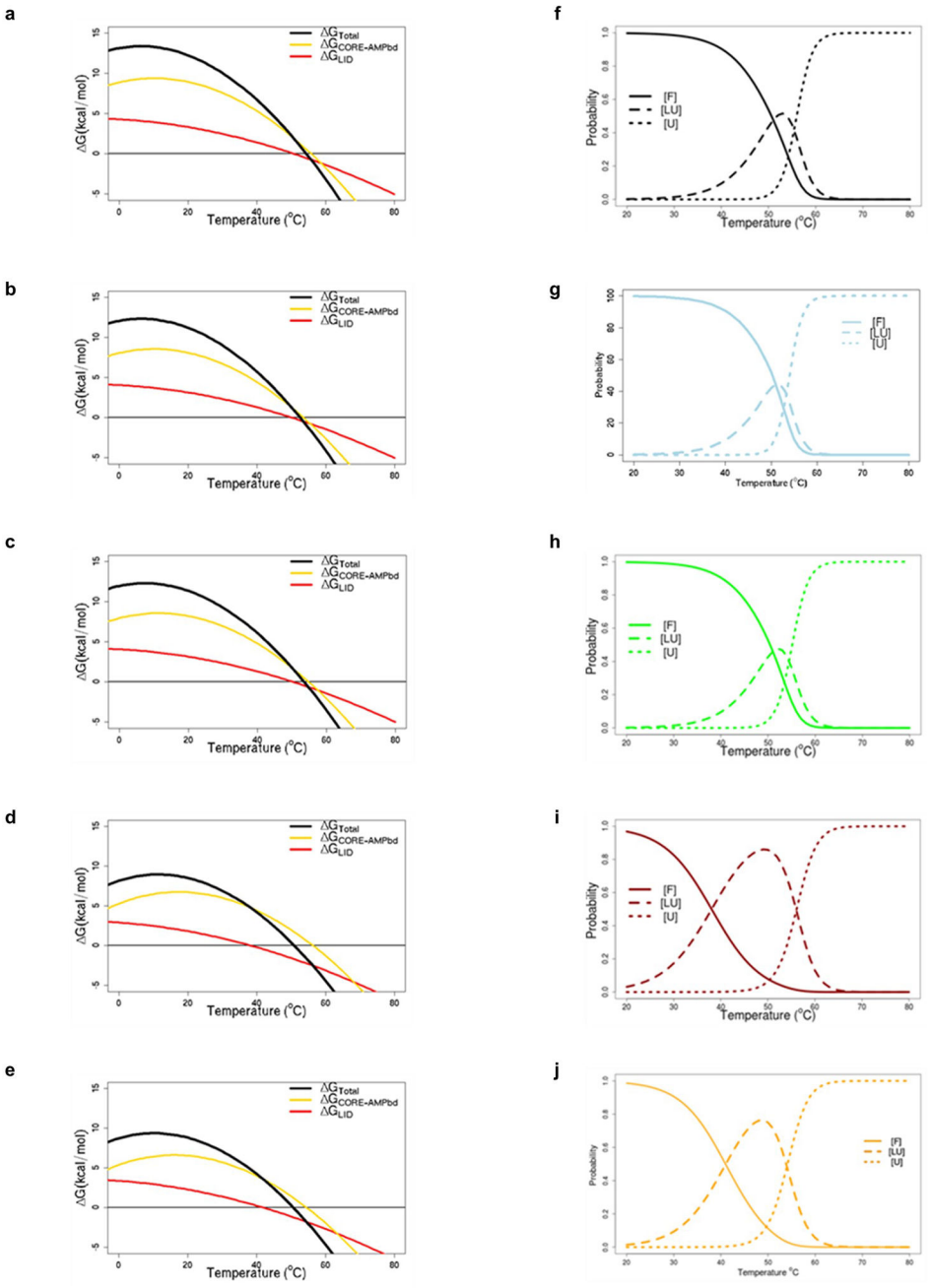

Extended Data Figure 5. Modeled domain stabilities and ensemble probabilities of AK variants

The DSC data for WT, *LID* and *AMPbd* mutants were each fit to 3-state transitions. The fitted parameters correspond to population profiles that differ dramatically between the *LID* and *AMPbd* mutants (Main Text figures 2b&c, respectively). As determined previously from circular dichroism and isothermal titration calorimetry (Schrank, 2009), the locally unfolded intermediate (LU), which is 5% populated at physiological temperature for WT AK (37°C), is increased to ~40% in the *LID* mutants (Main Text figure 2b). In contrast to the *LID*, mutations to the *AMPbd* do not stabilize the intermediate. Instead, the unfolded state (U) is stabilized, accounting for the decrease in the apparent T_m of the main peak, with no change

in the temperature of onset of the intermediate (Main Text figure 2c). **a. – e**. Representative domain stabilities calculated from DSC experiments, see Extended Data table 1. $\Delta G_{Total} = \Delta G_{CA} + \Delta G_{LID}$. Mutations other than those in the *LID* domain have a small impact on *AK* stability. **a**. WT **b**. A37G **c**. A55G **d**. V135G **e**. V142G. **f. – j**. Ensemble probability calculations were based on values found in Extended Data table 1. *LID* mutations V135G and V142G clearly modulate the ensemble by reducing the population of fully folded state and increasing population of unfolded *LID* domain. **f**. WT **g**. A37G **h**. A55G **i**. V135G **j**. V142G.

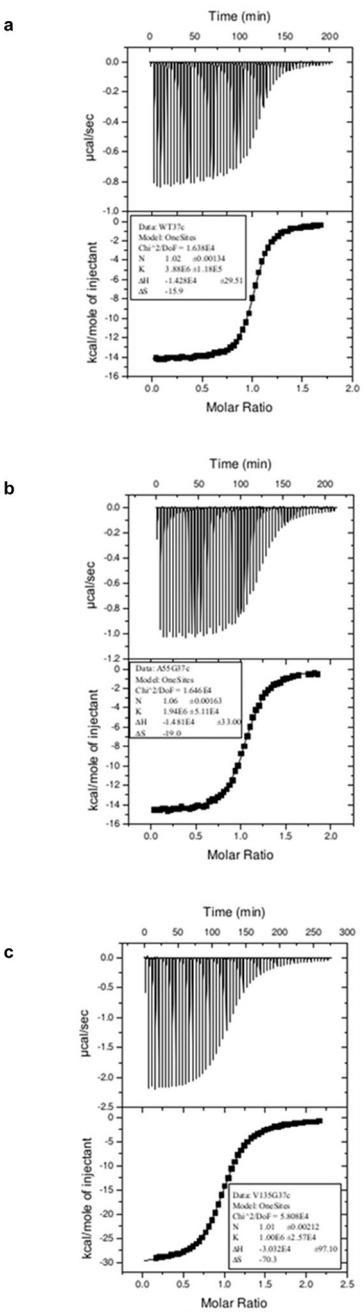

Extended Data Figure 6. Representative isothermal titration calorimetry data

All measurements were obtained at 37 °C, fitting parameters are indicated in each panel. Results represent $n = 1$ independent experiments. **a**. WT **b**. A55G **c**. V135G

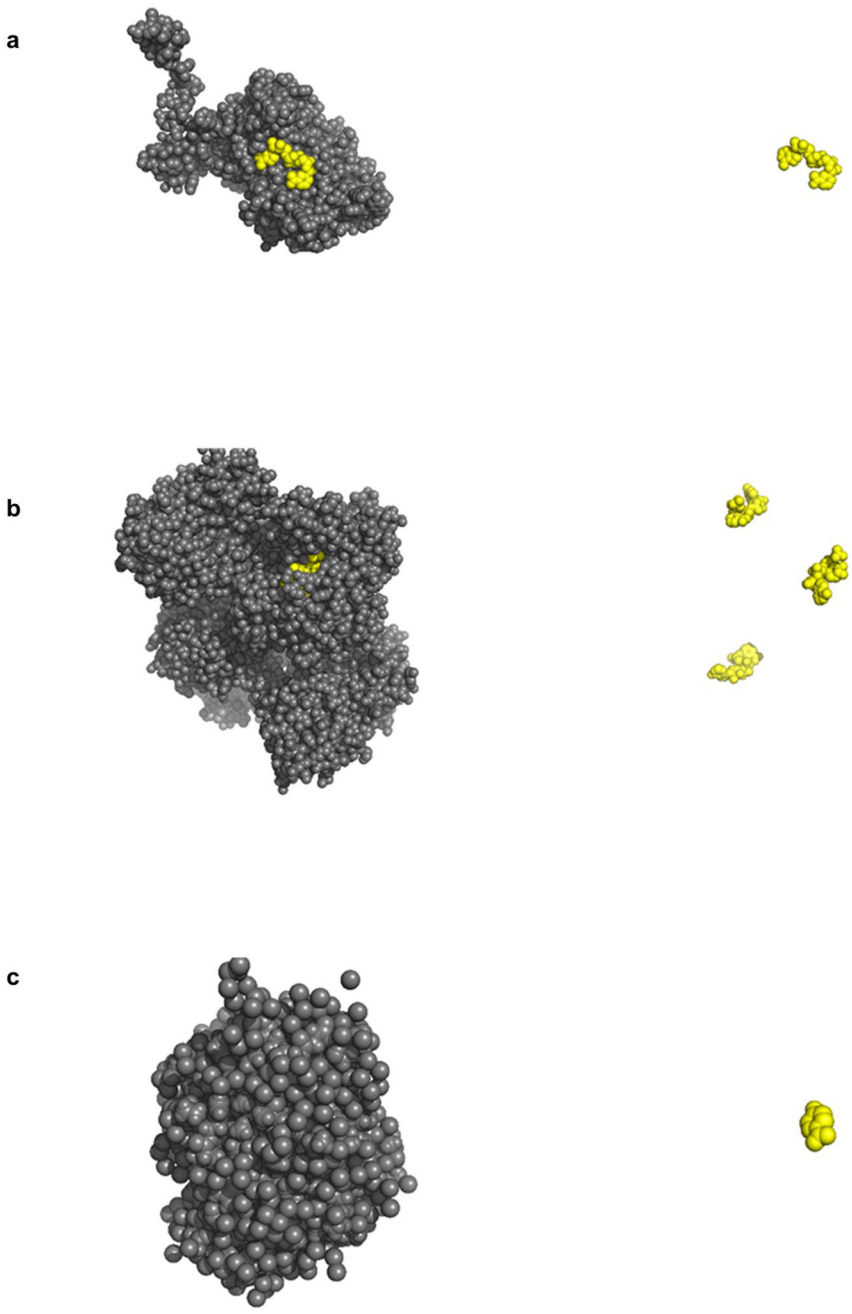

Extended Data Figure 7. Examples of *holo*-enzymes' degree of ligand burial

In each panel, atoms are shown as van der Waals' spheres. Dark gray indicates protein atoms and yellow indicates ligand. The left side of each panel shows the protein and ligand together, and the right side shows ligand alone. **a**. "Little" ligand surface area is buried in the complex of deoxyhypusine synthase and nicotinamide adenine-dinucleotide inhibitor, PDB identifier 1rlz. **b**. "Partial" ligand surface area is buried in the complex of glyceraldehyde-3-

phosphate dehydrogenase, nicotinamide adenine-dinucleotide cofactor, and glyceraldehyde-3-phosphate substrate, PDB identifier 1nqa. **c**. “Mostly” ligand surface area is buried in the complex of chorismate-pyruvate lyase and *p*-hydroxybenzoic acid product, PDB identifier 1tt8.

Extended Data Table 1

Summary of thermodynamic parameters obtained from DSC.

AK Variant	$T_{m,LID}$ [*] (°C)	$\Delta H_{vH,LID}$ (kcal/mol)	$\Delta C_{p,LID}$ (kcal/mol K)	$T_{m,CA}$ (°C)	$\Delta H_{vH,CA}$ (kcal/mol)	$\Delta C_{p,CA}$ (kcal/mol K)	$\Delta G_{Total,37°C}$ [†] (kcal/mol)
WT	50.7 ± 0.1[‡]	46.0 ± 0.3	0.7 ± 0.1	55.8 ± 0.1	132.3 ± 1.5	2.7 ± 0.4	7.8 ± 0.2
A37G	50.0 ± 0.1	44.5 ± 0.1	0.7 ± 0.1	53.5 ± 0.1	125.7 ± 0.6	2.7 ± 0.4	**6.8 ± 0.2**
A55G	50.2 ± 0.1	44.5 ± 0.1	0.7 ± 0.1	54.8 ± 0.1	126.0 ± 0.1	2.7 ± 0.4	**7.1 ± 0.2**
V135G	**38.1 ± 0.1** [§]	**37.4 ± 0.6**	0.7 ± 0.1	56.3 ± 0.1	**111.7 ± 0.1**	2.7 ± 0.4	**5.1 ± 0.3**
V142G	**41.8 ± 0.1**	**40.6 ± 1.5**	0.7 ± 0.1	54.5 ± 0.1	**110.3 ± 0.3**	2.7 ± 0.4	**5.2 ± 0.2**

[*] “*LID*” is abbreviation for “*Intermediate, Binding-Incompetent LID domain unfolding transition*”, “*CA*” for “*CORE-AMPbd domains unfolding transition*”, “WT” for “wild-type”, “vH” for “van‘t Hoff”.

[†] $\Delta G_{Total} = \Delta G_{LID} + \Delta G_{CA}$.

[‡] Values represent averages and standard deviations of three replicates.

[§] Values in **boldface** differ substantially from WT.

Supplementary Material

Refer to Web version on PubMed Central for supplementary material.

Acknowledgments

The authors thank Drs. Ananya Mujamdar (JHU NMR Core Facility) and Katie Tripp (JHU Center for Molecular Biophysics) for technical assistance and instrumentation. Funding from NIH (R01-GM063747), NSF (MCB-1330211), and Johns Hopkins University is acknowledged.

References

1. Beers JM, Jayasundara N. Antarctic notothenioid fish: what are the future consequences of 'losses' and 'gains' acquired during long-term evolution at cold and stable temperatures? J Exp Biol. 2015; 218:1834–1845. DOI: 10.1242/jeb.116129 [PubMed: 26085661]
2. Tattersall, Gv, et al. Coping with thermal challenges: physiological adaptations to environmental temperatures. Compr Physiol. 2012; 2:2151–2202. DOI: 10.1002/cphy.c110055 [PubMed: 23723035]
3. Fersht, AR. Enzyme Structure and Mechanism. WH Freeman; 1977.
4. Elias M, Wieczorek G, Rosenne S, Tawfik DS. The universality of enzymatic rate-temperature dependency. Trends Biochem Sci. 2014; 39:1–7. DOI: 10.1016/j.tibs.2013.11.001 [PubMed: 24315123]
5. Somero GN. Adaptation of enzymes to temperature: searching for basic "strategies". Comp Biochem Physiol B Biochem Mol Biol. 2004; 139:321–333. DOI: 10.1016/j.cbpc.2004.05.003 [PubMed: 15544958]
6. Fields PA, Somero GN. Hot spots in cold adaptation: localized increases in conformational flexibility in lactate dehydrogenase A4 orthologs of Antarctic notothenioid fishes. Proceedings of the National Academy of Sciences of the United States of America. 1998; 95:11476–11481. [PubMed: 9736762]

7. Fields PA, Dong Y, Meng X, Somero GN. Adaptations of protein structure and function to temperature: there is more than one way to 'skin a cat'. J Exp Biol. 2015; 218:1801–1811. DOI: 10.1242/jeb.114298 [PubMed: 26085658]
8. Henzler-Wildman KA, et al. Intrinsic motions along an enzymatic reaction trajectory. Nature. 2007; 450:838–844. [PubMed: 18026086]
9. Aden J, Verma A, Schug A, Wolf-Watz M. Modulation of a pre-existing conformational equilibrium tunes adenylate kinase activity. J Am Chem Soc. 2012; 134:16562–16570. DOI: 10.1021/ja3032482 [PubMed: 22963267]
10. Counago R, Shamoo Y. Gene replacement of adenylate kinase in the gram-positive thermophile Geobacillus stearothermophilus disrupts adenine nucleotide homeostasis and reduces cell viability. Extremophiles. 2005; 9:135–144. [PubMed: 15647886]
11. Rundqvist L, et al. Noncooperative folding of subdomains in adenylate kinase. Biochemistry. 2009; 48:1911–1927. [PubMed: 19219996]
12. Kerns SJ, et al. The energy landscape of adenylate kinase during catalysis. Nat Struct Mol Biol. 2015; 22:124–131. DOI: 10.1038/nsmb.2941 [PubMed: 25580578]
13. Beckstein O, Denning EJ, Perilla JR, Woolf TB. Zipping and unzipping of adenylate kinase: atomistic insights into the ensemble of open<-->closed transitions. Journal of molecular biology. 2009; 394:160–176. DOI: 10.1016/j.jmb.2009.09.009 [PubMed: 19751742]
14. Daily MD, Makowski L, Phillips GN Jr, Cui Q. Large-scale motions in the adenylate kinase solution ensemble: coarse-grained simulations and comparison with solution X-ray scattering. Chem Phys. 2012; 396:84–91. DOI: 10.1016/j.chemphys.2011.08.015 [PubMed: 22711968]
15. Schrank TP, Bolen DW, Hilser VJ. Rational modulation of conformational fluctuations in adenylate kinase reveals a local unfolding mechanism for allostery and functional adaptation in proteins. Proceedings of the National Academy of Sciences of the United States of America. 2009; 106:16984–16989. DOI: 10.1073/pnas.0906510106 [PubMed: 19805185]
16. Schrank TP, Wrabl JO, Hilser VJ. Conformational Heterogeneity Within the LID Domain Mediates Substrate Binding to Escherichia coli Adenylate Kinase: Function Follows Fluctuations. Dynamics in Enzyme Catalysis. 2013; 337:95–121. DOI: 10.1007/128_2012_410
17. Olsson U, Wolf-Watz M. Overlap between folding and functional energy landscapes for adenylate kinase conformational change. Nature communications. 2010; 1:111.
18. Rogne P, Wolf-Watz M. Urea-Dependent Adenylate Kinase Activation following Redistribution of Structural States. Biophys J. 2016; 111:1385–1395. DOI: 10.1016/j.bpj.2016.08.028 [PubMed: 27705762]
19. D'Aquino JA, et al. The magnitude of the backbone conformational entropy change in protein folding. Proteins. 1996; 25:143–156. DOI: 10.1002/(SICI)1097-0134(199606)25:2<143::AID-PROT1>3.0.CO;2-J [PubMed: 8811731]
20. Schrank TP, Elam WA, Li J, Hilser VJ. Strategies for the thermodynamic characterization of linked binding/local folding reactions within the native state application to the LID domain of adenylate kinase from Escherichia coli. Methods in enzymology. 2011; 492:253–282. DOI: 10.1016/B978-0-12-381268-1.00020-3 [PubMed: 21333795]
21. Henzler-Wildman KA, et al. A hierarchy of timescales in protein dynamics is linked to enzyme catalysis. Nature. 2007; 450:913–916. DOI: 10.1038/nature06407 [PubMed: 18026087]
22. Wolf-Watz M, et al. Linkage between dynamics and catalysis in a thermophilic-mesophilic enzyme pair. Nature Structural and Molecular Biology. 2004; 11:945–949.
23. Hansen DF, Vallurupalli P, Kay LE. An improved 15N relaxation dispersion experiment for the measurement of millisecond time-scale dynamics in proteins. J Phys Chem B. 2008; 112:5898–5904. DOI: 10.1021/jp074793o [PubMed: 18001083]
24. Palmer AG, Kroenke CD, Loria JP. Nuclear magnetic resonance methods for quantifying microsecond-to-millisecond motions in biological macromolecules. Methods in Enzymology. 2001; 339:204–238. [PubMed: 11462813]
25. Eyring H. The activated complex in chemical reactions. Journal of Chemical Physics. 1935; 3:107–114.
26. Warshel A, Bora RP. Perspective: Defining and quantifying the role of dynamics in enzyme catalysis. J Chem Phys. 2016; 144:180901. [PubMed: 27179464]

27. Nguyen V, et al. Evolutionary drivers of thermoadaptation in enzyme catalysis. Science. 2017; 355:289–294. DOI: 10.1126/science.aah3717 [PubMed: 28008087]
28. Arrhenius, S. Textbook of Electrochemistry. Longmans, Green and Co; 1902.
29. Siddiqui KS. Defying the activity-stability trade-off in enzymes: taking advantage of entropy to enhance activity and thermostability. Crit Rev Biotechnol. 2017; 37:309–322. DOI: 10.3109/07388551.2016.1144045 [PubMed: 26940154]
30. Kim YE, Hipp MS, Bracher A, Hayer-Hartl M, Hartl FU. Molecular chaperone functions in protein folding and proteostasis. Annu Rev Biochem. 2013; 82:323–355. DOI: 10.1146/annurev-biochem-060208-092442 [PubMed: 23746257]
31. Muller CW, Schlauderer GJ, Reinstein J, Schulz GE. Adenylate kinase motions during catalysis: an energetic counterweight balancing substrate binding. Structure. 1996; 4:147–156. [PubMed: 8805521]
32. Muller CW, Schulz GE. Structure of the complex between adenylate kinase from Escherichia coli and the inhibitor Ap5A refined at 1.9 A resolution. A model for a catalytic transition state. Journal of molecular biology. 1992; 224:159–177. [PubMed: 1548697]
33. Schrank TP, Bolen DW, Hilser VJ. Rational modulation of conformational fluctuations in adenylate kinase reveals a local unfolding mechanism for allostery and functional adaptation in proteins. Proceedings of the National Academy of Sciences of the United States of America. 2009; 106:16984–16989. DOI: 10.1073/pnas.0906510106 [PubMed: 19805185]
34. Rhoads DG, Lowenstein JM. Initial velocity and equilibrium kinetics of myokinase. The Journal of biological chemistry. 1968; 243:3963–3972. [PubMed: 5690818]
35. Eyring H. The activated complex in chemical reactions. Journal of Chemical Physics. 1935; 3:107–114.
36. Laidler KJ, King MC. The development of transition state theory. Journal of Physical Chemistry. 1983; 87:2657–2664.
37. Murray V, Huang YF, Chen JL, Wang JJ, Li QQ. A Novel Bacterial Expression Method with Optimized Parameters for Very High Yield Production of Triple-Labeled Proteins. Methods Mol Biol. 2012; 831:1–18. DOI: 10.1007/978-1-61779-480-3_1 [PubMed: 22167665]
38. Schrank TP, Wrabl JO, Hilser VJ. Conformational Heterogeneity Within the LID Domain Mediates Substrate Binding to Escherichia coli Adenylate Kinase: Function Follows Fluctuations. Dynamics in Enzyme Catalysis. 2013; 337:95–121. DOI: 10.1007/128_2012_410
39. Hansen DF, Vallurupalli P, Kay LE. An improved 15N relaxation dispersion experiment for the measurement of millisecond time-scale dynamics in proteins. J Phys Chem B. 2008; 112:5898–5904. DOI: 10.1021/jp074793o [PubMed: 18001083]
40. Lisi GP, Loria JP. Solution NMR Spectroscopy for the Study of Enzyme Allostery. Chem Rev. 2016; 116:6323–6369. DOI: 10.1021/acs.chemrev.5b00541 [PubMed: 26734986]
41. Hilser VJ, Wrabl JO, Motlagh H. Structural and energetic basis of allostery. Annual Reviews of Biophysics. 2012; 41:585–609.

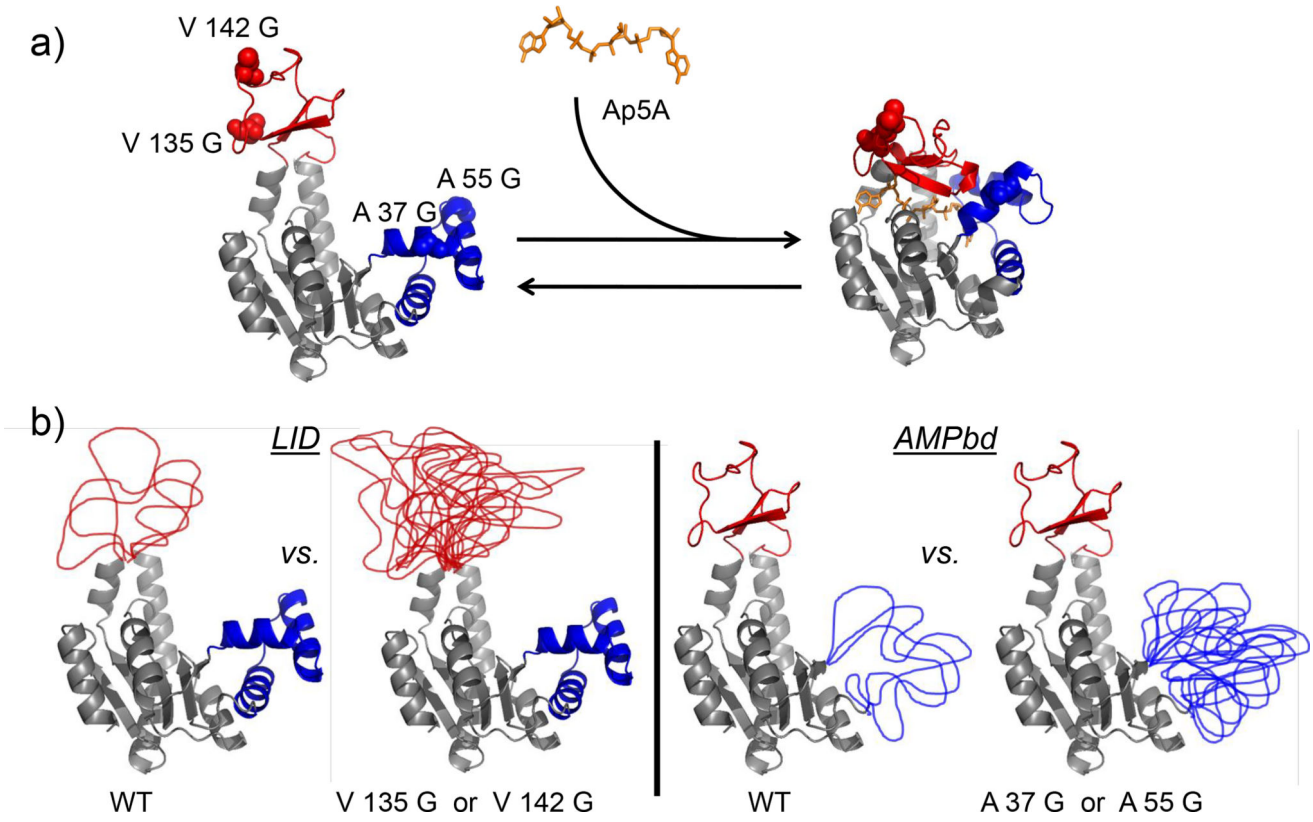

Figure 1. Domain structure of *E. coli* AK and sites of allosteric entropy-tuning mutations

a) Two crystallographically identified states are “Open” (left, 4ake.pdb) and “Closed” (right 1ake.pdb) with substrate analog Ap5A. Domains and mutation sites in color: *CORE* gray, *AMPbd* blue, *LID* red. b) Entropy-enhancing Gly mutations. Changes from Val to Gly in the *LID* (left) and Ala to Gly in the *AMPbd* (right) are visually quantified by amounts of locally unfolded conformations.

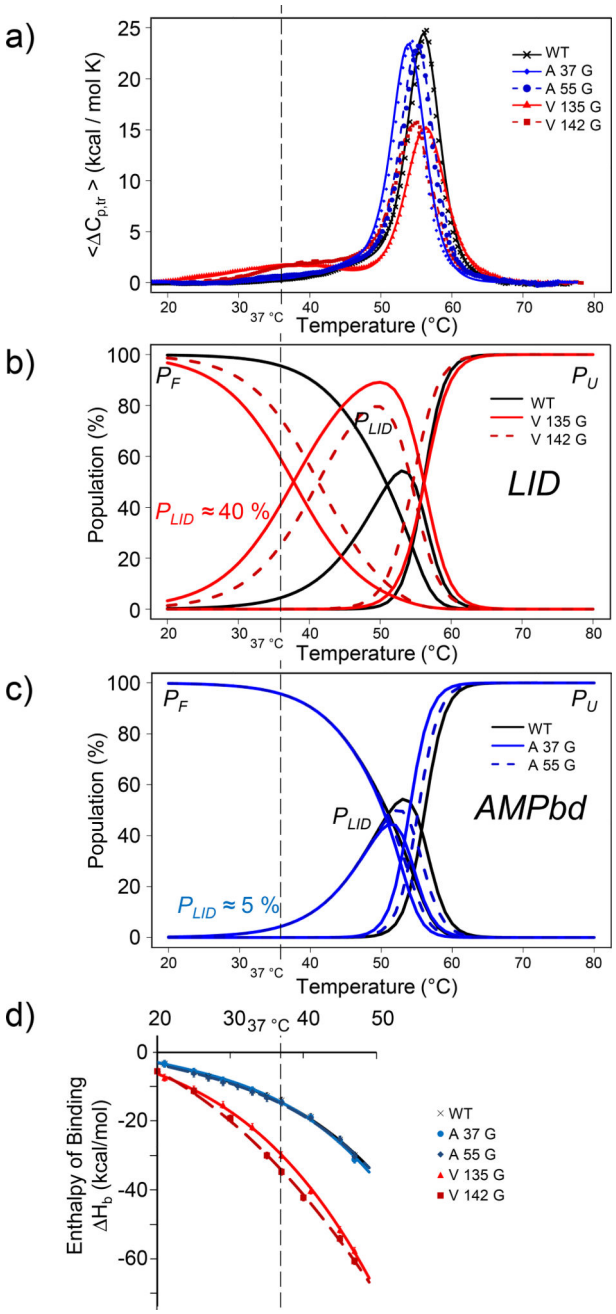

Figure 2. Thermodynamics of conformational fluctuations in *LID* and *AMPbd* entropy-enhancing mutants

a) DSC unfolding data. WT in black; red and blue colors respectively show mutations in *LID* and *AMPbd*. Smooth curves are best fits to equation (S7). b) Populations of major conformational states. Values obtained from equation (S10) using values in Extended Data table 1. At physiological temperature of 37 °C, (vertical dashed lines) mutants populate *LID* unfolded state P_{LID}. c) Populations of major conformational states. At 37 °C, populations of folded WT and both mutants were similar at 95%. d) ITC binding enthalpies. Smooth curves are polynomials to guide the eye. Data converge at low temperature, corroborating the

observation that mutations do not perturb the WT structure. Results represent $n = 1$ independent experiments.

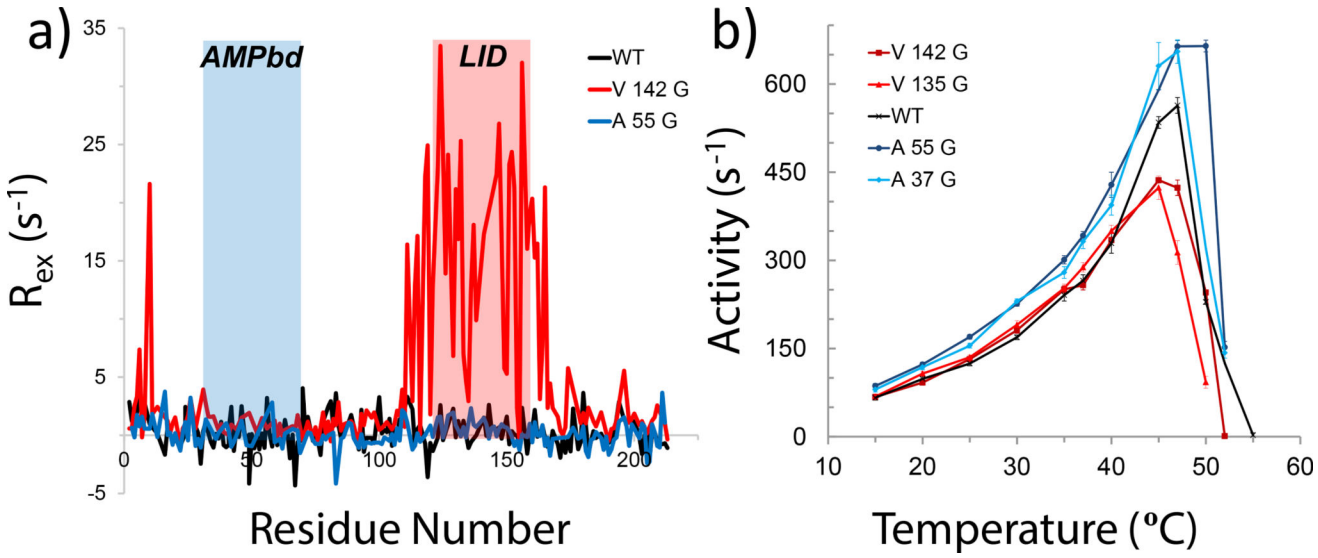

Figure 3. NMR relaxation-dispersion dynamics and enzyme activity of *LID and AMPbd* are independent

a) Position-specific conformational exchange rates R_{ex} at 19 °C. Rates for *LID* mutation V142G *vs.* WT show increased fluctuations in *LID* residues 110–160, while rates for *AMPbd* mutation A55G exhibit fluctuations comparable to WT. Results represent $n = 1$ independent experiments. b) Activities as a function of temperature. Rollover due to protein denaturation occurs at higher temperature (> 45 °C). Results represent mean +/− s. d. of $n =$ 3 independent experiments.

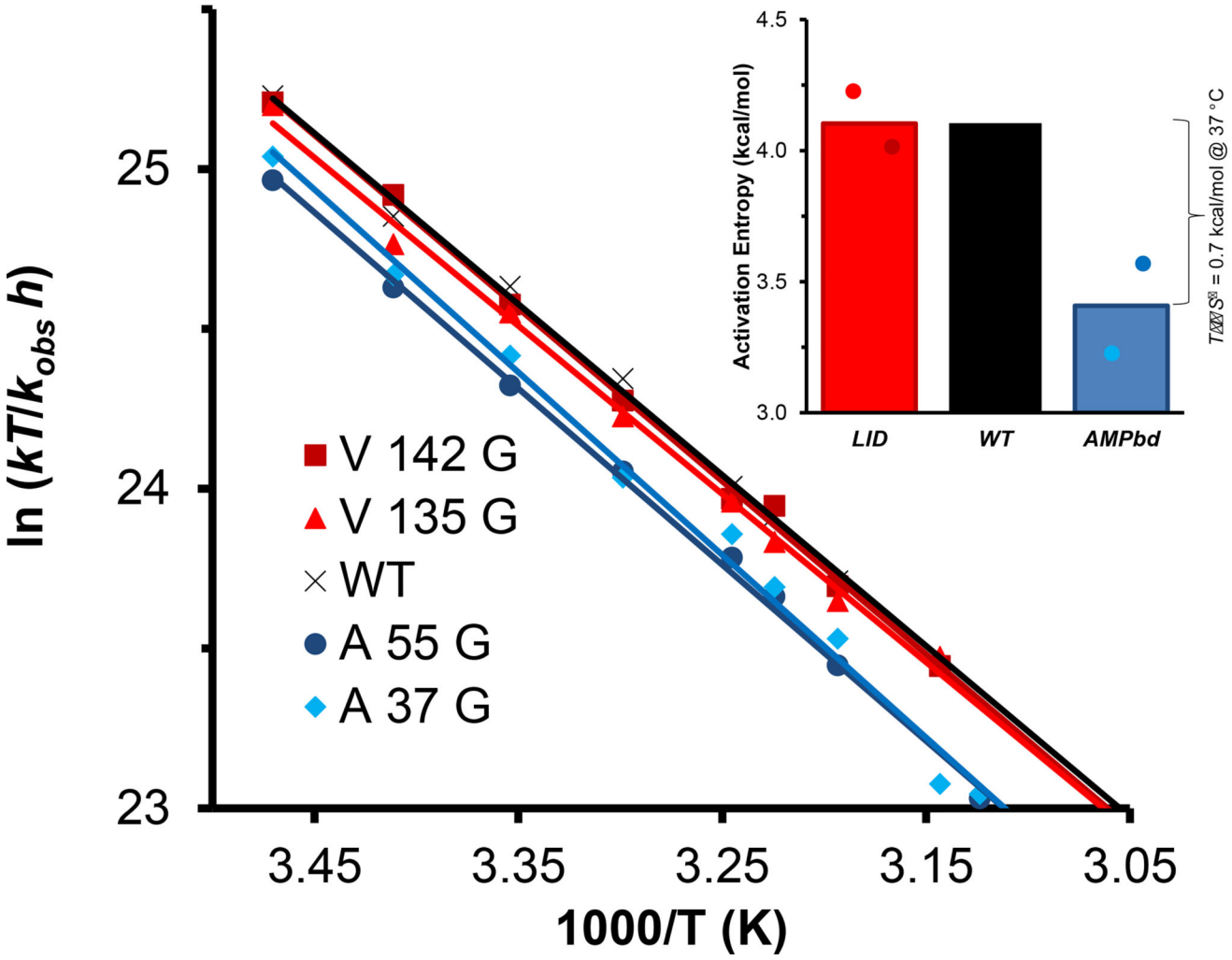

Figure 4. Eyring plots of enzyme activity

LID mutations (red) do not deviate significantly from WT (black); *AMPbd* mutations have lower activation energy and are more active at all temperatures. Intercepts, converted to activation entropies (inset), are similar between the *LID* mutants and WT. Values and error bars are average and standard deviation of two mutations. Measured catalytic rate is represented by k_{obs}, T is temperature, k and h, respectively, are Boltzmann and Planck constants. All Pearson correlations exhibited R^2 values ≥ 0.992, with [slope, intercept] as follows: WT [5348.2, 6.6612], A37G [5716.4, 5.2145], A55G [5313.0, 5.8448], V135G [5261.4, 6.8835], V142G [5412.2, 6.4336]. Bars represent the mean of the two indicated points.

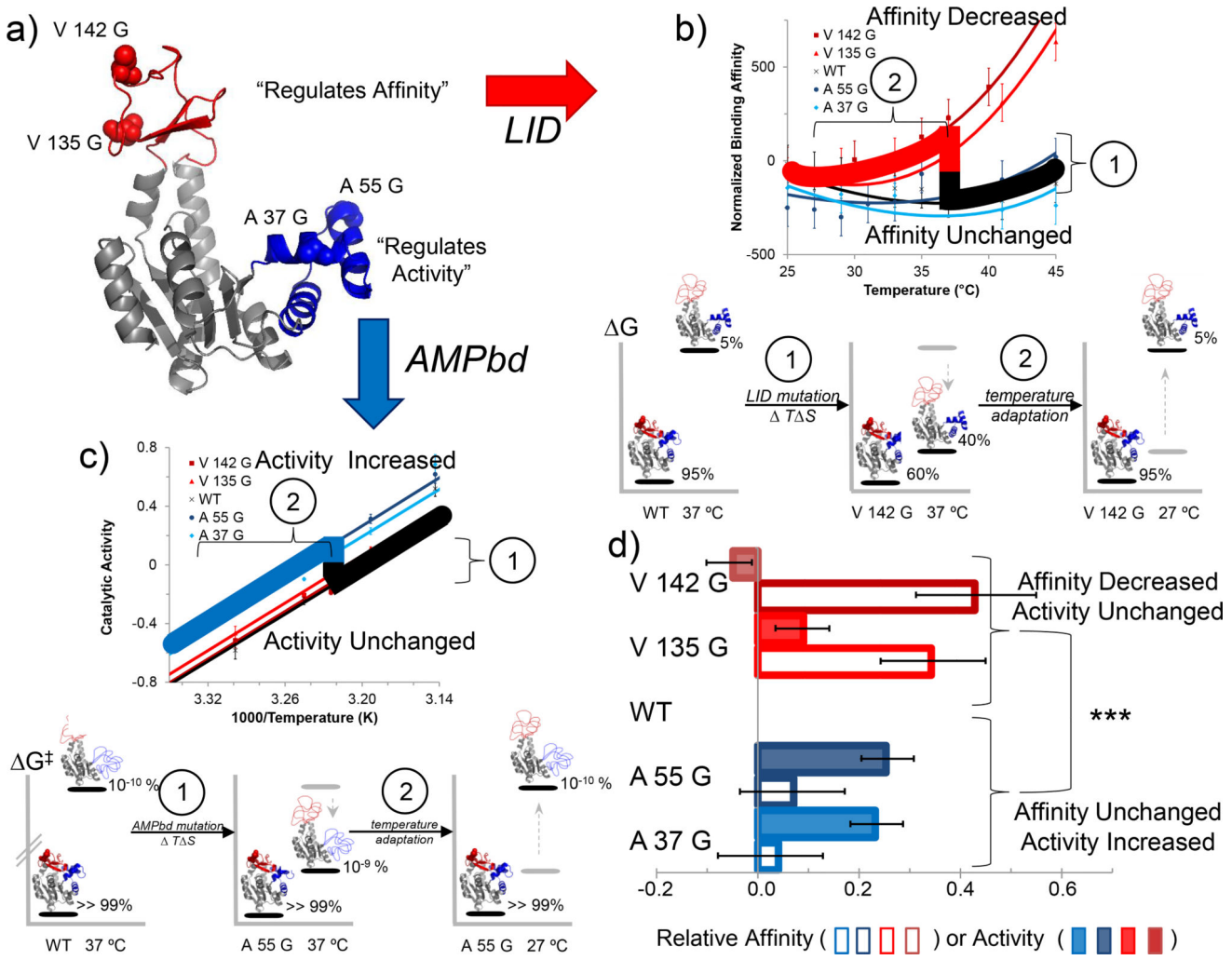

Figure 5. Spatially segregated tunability of cold adaptation

a) Locations of entropy-enhancing mutations reveal affinity – activity decoupling. *LID* (red arrow) regulates binding and *AMPbd* (blue arrow) regulates turnover. Results represent mean +/− s.d. of $n = 3$ independent experiments. b) Binding affinity (y-axis) units are cal/mol, normalized within each mutant to reference temperature of 19 °C. Results represent mean +/− s.d. of $n = 3$ independent experiments. c) Enzyme activity (y-axis) is expressed as $\ln(k_{cat}/T)$, where T is Kelvin and k_{cat} is 1/s. Energy levels and populations of *LID* (figure 5b) or *AMPbd* (figure 5c) are shown under each cartoon molecule. Single Gly mutations independently perturb the locally unfolded population of each domain (Step 1, circled), controlling binding (*in the case of LID*) or activity (*in the case of AMPbd*). Temperature adaptation of the enzyme (Step 2, circled) is effected by resetting the functional temperature (thick black-to-red or black-to-blue lines). Conformational entropy adjusts populations of binding-competent or product-release states of AK such that functional change is minimized over a 5 °C – 10 °C temperature differential (before and after Step 2). d) Selective domain-specific modulation of activity and affinity at physiological temperature. Values from panels b and c are scaled by WT AK values at 37 °C. Relative binding affinity, $\Delta\Delta G_b^*$, is defined as the 37 °C value from panel b for *WT* subtracted from the mutant value, *i.e.* ($\Delta G_{b,mut,37\ °C}$

$-\Delta G_{b,mut,19\,°C})-(\Delta G_{b,mut,37\,°C}-\Delta G_{b,mut,19\,°C})$; shown as unfilled bars in units of kcal/mol on the x-axis. Relative activity, Δk_{cat}^{*}, is defined as unitless ratio $\ln[(k_{cat,mut,37\,°C} - k_{cat,mut,19\,°C})/(kcat_{wt,37\,°C} - k_{cat,wt,19\,°C})]$. Larger x-axis values simultaneously indicate decreased binding affinity (unfilled bars) and increased activity (filled bars). Entropy-enhancing Gly mutants in *LID* (red) decrease affinity without changing activity, while mutants in *AMPbd* (blue) increase activity without changing affinity. Bars represent the difference of averages from $n = 3$ independent experiments, error bars represent difference propagation of s.d. of the independent experiments. Asterisks indicate significance of $p = 0.00015$ from Event Tree Analysis, assuming that each of the eight non-*WT* measurements could independently increase, decrease, or remain unchanged relative to *WT* ($3^8 = 6561$ possibilities).